

# Upper limit set by causality on the tidal deformability of a neutron star

Eric D. Van Oeveren and John L. Friedman

*Leonard E. Parker Center for Gravitation,*

*Cosmology and Astrophysics*

*University of Wisconsin-Milwaukee*

*3135 N Maryland Ave,*

*Milwaukee, WI 53211, USA*

## Abstract

A principal goal of gravitational-wave astronomy is to constrain the neutron star equation of state (EOS) by measuring the tidal deformability of neutron stars. The tidally induced departure of the waveform from that of point-particle (or spinless binary black hole (BBH)) increases with the stiffness of the EOS. We show that causality (the requirement that the speed of sound is less than the speed of light for a perfect fluid satisfying a one-parameter equation of state) places an upper bound on tidal deformability as a function of mass. Like the upper mass limit, the limit on deformability is obtained by using an EOS with  $v_{\text{sound}} = c$  for high densities and matching to a low density (candidate) EOS at a matching density of order nuclear saturation density. We use these results and those of [B.D. Lackey *et al.*, Phys. Rev. D **89**, 043009 (2014)] to estimate the resulting upper limit on the gravitational-wave phase shift of a black hole-neutron star (BHNS) binary relative to a BBH. Even for assumptions weak enough to allow a maximum mass of  $4M_{\odot}$  (a match at nuclear saturation density to an unusually stiff low-density candidate EOS), the upper limit on dimensionless tidal deformability is stringent. It leads to a still more stringent estimated upper limit on the maximum tidally induced phase shift prior to merger. We comment in an appendix on the relation between causality, the condition  $v_{\text{sound}} < c$ , and the condition  $dp/d\epsilon < 1$  for the effective EOS governing the equilibrium star.

## I. INTRODUCTION

As the second generation of ground-based interferometric gravitational wave detectors (Advanced LIGO, Advanced Virgo, KAGRA, and LIGO-India) approach design sensitivity, we are likely to detect each year the inspiral and coalescence of several compact binary systems that include neutron stars, both BHNS and binary neutron-star (BNS) systems. These observations can constrain the neutron-star equation of state (EOS), which gives the pressure  $p$  in terms of the energy density  $\epsilon$ . A stiffer EOS, where the pressure increases rapidly with density, yields stars with larger radii and larger tidal effects on the waveform, governed by the star's *tidal deformability*. In particular, tidal distortion during inspiral increases with the stiffness of the equations of state. Because energy is lost both to gravitational waves and to the work needed to distort the stars, the inspiral proceeds more rapidly for stars with greater tidal deformability. The result is a waveform in which the increase in frequency is more rapid and in which coalescence occurs sooner – at lower frequency.

Beginning with work by Kochanek [1] and Lai and Wiseman [2], a number of authors have studied the effect of tides on inspiral waveforms. Simulations [3–21] of BHNS and BNS systems and analytic approximations in the context of post-Newtonian theory [22] and the Effective-One-Body (EOB) formalism [23–25] are nearing the precision needed to extract neutron-star deformability from observations with the projected sensitivity of Advanced LIGO. Recent estimates of the measurability of tidal effects and the ability of these observatories to constrain the EOS with signals from BHNS and BNS systems are given in [26–30] and references therein.

In this work, we obtain the upper limit imposed by causality on the tidal deformability of neutron stars and estimate the resulting constraint on the maximum departure of the waveform of a BHNS inspiral from a corresponding spinless BBH inspiral. The limit is analogous to the upper limits on neutron-star mass  $M_{NS}$  [31, 32] and radius  $R$  [33]. In each case, one assumes an EOS of the form  $p = p(\epsilon)$  that is known below an energy density  $\epsilon_{\text{match}}$ , and one obtains a limit on  $M$  and  $R$  by requiring that the EOS be causal for  $\epsilon > \epsilon_{\text{match}}$  in the sense that the sound speed, given by  $\sqrt{dp/d\epsilon}$ , must be less than the speed of light. Because the sound speed is a measure of the stiffness of the EOS, this is a constraint on the stiffness. An upper limit on tidal deformability then implies an upper limit on the departure of gravitational wave phase shifts from corresponding waveforms of BBH inspiral.

We use metric signature  $-+++$  and gravitational units with  $G = c = 1$ .

## II. METHOD

### A. Causal EOS

For a perfect fluid with a one-parameter EOS  $p = p(\epsilon)$ , causality implies that the speed of sound,  $\sqrt{dp/d\epsilon}$ , is less than the speed of light. That is, the dynamical equations describing the evolution of fluid and metric are hyperbolic, with characteristics associated with fluid degrees of freedom lying outside the light cone unless

$$\frac{dp}{d\epsilon} \leq 1. \quad (1)$$

There is some inaccuracy in using the one-parameter EOS that governs the equilibrium star to define the characteristic velocities of the fluid, because fluid oscillations with the highest velocities have frequencies too high for the temperature of a fluid element and the relative density  $Y_i$  of each species of particle to reach their values for the background fluid star. Nevertheless, using a result of Geroch and Lindblom [34], we show in Appendix A that causality implies the equilibrium inequality (1) for locally stable relativistic fluids satisfying a two-parameter EOS  $p = p(\epsilon, s)$ , where  $s$  is the entropy per baryon. For the multi-parameter equation of state  $\epsilon = \epsilon(p, s, Y_i)$ , with  $Y_i$  the relative density of each species of particle, one must assume without proof that causality implies  $v_{\text{sound}} < 1$ ; the equilibrium inequality (1) again follows from local stability.

The speed of sound is a measure of the stiffness of the EOS. The well-known upper limit on the mass of a neutron star and a corresponding upper limit on its radius are obtained by using the stiffest EOS consistent with causality and with an assumed known form at low density. That is, above a density  $\epsilon_{\text{match}}$ , the EOS is given by

$$\epsilon - \epsilon_{\text{match}} = p - p_{\text{match}}, \quad (2)$$

where  $p_{\text{match}}$  is fixed by continuity to be the value of  $p$  at  $\epsilon_{\text{match}}$  for the assumed low-density EOS. The upper limits on mass and radius are then found as functions of the matching density  $\epsilon_{\text{match}}$ .

In this work, we again use an EOS of this form to find an upper limit on neutron-star deformability. There is some remaining uncertainty in the EOS near nuclear saturation

density, and this has a larger impact on the deformability than on the maximum mass or radius because the deformability is roughly proportional to  $R^5$ . To be conservative, we choose the MS1 EOS [35], which is among the stiffest candidate equations of state for  $\epsilon \lesssim \epsilon_{\text{nuc}}$ . Our *matched causal EOS* is then given by

$$p(\epsilon) = \begin{cases} p_{\text{MS1}}(\epsilon), & \epsilon \leq \epsilon_{\text{match}} \\ \epsilon - \epsilon_{\text{match}} + p_{\text{MS1}}(\epsilon_{\text{match}}), & \epsilon \geq \epsilon_{\text{match}}. \end{cases} \quad (3)$$

In computing the deformability, we consider only irrotational neutron stars; and in estimating the effect of tides on the inspiral phase, we neglect resonant coupling of tides to neutron-star modes. Tidal deformation of slowly rotating relativistic stars is treated by Pani *et al.* [36]; and Essick *et al.* [37] argue that tidal excitation of coupled modes may alter the waveform in BNS systems.

## B. Static, Spherical Stars

We next construct the sequence of static spherical stars based on the causal EOS (3). We numerically integrate the Tolman-Oppenheimer-Volkoff (TOV) equation [38],

$$\left(1 - \frac{2m}{r}\right) \frac{dp}{dr} = -\frac{1}{r^2}(\epsilon + p)(m + 4\pi r^3 p), \quad (4)$$

where  $m(r)$  is the total mass-energy inside radius  $r$ , related to  $\epsilon$  by

$$\frac{dm}{dr} = 4\pi r^2 \epsilon. \quad (5)$$

A member of the sequence is specified by its central density  $\epsilon_c$ . Its circumferential radius  $R$  is the value of the Schwarzschild coordinate  $r$  at which  $p(r) = 0$ , and its gravitational mass is  $M = m(R)$ .

## C. Calculating the Tidal Deformability

The departure of the inspiral of a BHNS binary from point-particle (or spinless BBH) inspiral depends on the tidal deformation of the neutron star due to the tidal field of its companion. For large binary separation, the metric near the neutron star can be written as a linear perturbation of the Schwarzschild metric of the unperturbed star that has two

parts: The tidal field of the companion, expressed in Schwarzschild coordinates about the center of mass of the neutron star, has the form of an external quadrupole field; and the induced quadrupole distortion of the neutron star gives a second quadrupole contribution to the perturbed metric. That is, outside the support of the star, the quadrupole perturbation is a sum,

$$\delta g_{\alpha\beta} = \delta_{\text{external}} g_{\alpha\beta} + \delta_{\text{induced}} g_{\alpha\beta}, \quad (6)$$

of two time-independent solutions to the field equations linearized about a vacuum Schwarzschild geometry. In a gauge associated with asymptotically Cartesian and mass centered coordinates, the contributions to the perturbed metric have the form

$$\delta_{\text{external}} g_{tt} = -r^2 \mathcal{E}_{ij} n^i n^j + \mathcal{O}(r), \quad (7)$$

with no  $r^{-3}$  contribution, and

$$\delta_{\text{induced}} g_{tt} = \frac{3}{r^3} Q_{ij} \left( n^i n^j - \frac{1}{3} \delta^{ij} \right) + \mathcal{O}(r^{-4}). \quad (8)$$

Here  $n^i = x^i/r$  is an outward-pointing unit vector,  $\mathcal{E}_{ij} \propto M_{\text{BH}}/r_{\text{BHNS}}^3$  is the tracefree tidal field from the black hole, and  $Q_{ij}$  is the neutron star's induced quadrupole moment. The quadrupole moment tensor  $Q_{ij}$  is proportional to  $\mathcal{E}_{ij}$ ,

$$Q_{ij} = -\lambda \mathcal{E}_{ij}, \quad (9)$$

and the constant of proportionality  $\lambda$  is the *tidal deformability* of the neutron star. It measures the magnitude of the quadrupole moment induced by an external tidal field and is proportional to the (dimensionless)  $\ell = 2$  tidal Love number [39]

$$k_2 = \frac{3\lambda}{2R^5}. \quad (10)$$

After constructing the one-parameter family of spherical stars satisfying Eqs. (3), (4), and (5), we tidally perturb them, compute  $k_2$  and the radius  $R$  of each star, and then find the tidal deformability  $\lambda$  from Eq. (10). To calculate  $k_2$ , we use the method described by Hinderer [40]: A perturbation of the spherically symmetric background metric

$$\mathbf{g} = -e^{2\nu} dt^2 + \frac{1}{1 - 2m/r} dr^2 + r^2 (d\theta^2 + \sin^2 \theta d\phi^2), \quad (11)$$

with  $\nu(r)$  determined by

$$\left( 1 - \frac{2m}{r} \right) \frac{d\nu}{dr} = \frac{1}{r^2} (m + 4\pi r^3 p),$$

is found in the Regge-Wheeler gauge [41], with  $\delta\mathbf{g}$  a linear, quadrupolar, static, polar-parity perturbation given by [40]<sup>1</sup>

$$\delta\mathbf{g} = (-e^{2\nu} dt^2 + \frac{1}{1-2m/r} dr^2) H Y_{2,m}(\theta, \phi) + r^2 (d\theta^2 + \sin^2 \theta d\phi^2) K Y_{2,m}(\theta, \phi), \quad (12)$$

where  $H$  and  $K$  are both functions of  $r$ . The perturbed Einstein equation gives a differential equation for  $H$  [40]:

$$\begin{aligned} & \frac{d^2 H}{dr^2} \left(1 - \frac{2m}{r}\right) + \frac{dH}{dr} \left[\frac{2}{r} - \frac{2m}{r^2} + 4\pi r(p - \epsilon)\right] + \\ & H \left[-\frac{6}{r^2} + 4\pi \left(5\epsilon + 9p + \frac{\epsilon + p}{dp/d\epsilon}\right) - 4 \left(1 - \frac{2m}{r}\right) \left(\frac{d\nu}{dr}\right)^2\right] = 0. \end{aligned}$$

In vacuum,  $H$  can be written as a linear combination of  $P_2^2(r/M-1)$  and  $Q_2^2(r/M-1)$ , where  $P_2^2$  and  $Q_2^2$  are the  $\ell = m = 2$  associated Legendre functions. When expanded in powers of  $M/r$  at infinity,  $P_2^2(r/M-1) = \mathcal{O}(M/r)^3$  and  $Q_2^2(r/M-1) = \mathcal{O}(r/M)^2$ . The coefficient of  $P_2^2$  is therefore related to the quadrupole moment of the star, and the coefficient of  $Q_2^2$  is related to the tidal field applied by the black hole. By matching  $H(r)$  and its derivative across the surface of the star, one can show [40]

$$\begin{aligned} k_2 = & \frac{8}{5} C^5 (1-2C)^2 [2 + 2C(Y-1) - Y] \cdot \\ & \{2C[6 - 3Y + 3C(5Y-8) + 2C^2(13-11Y) + 2C^3(3Y-2) + 4C^4(Y+1)] \\ & + 3(1-2C)^2 [2 - Y + 2C(Y-1)] \log(1-2C)\}^{-1}, \end{aligned} \quad (13)$$

where  $C = M_{\text{NS}}/R$  is the compactness of the star,  $Y = RH'(R)/H(R)$ , and  $R$  is the radius of the star. Since  $k_2$  depends on  $Y$  and not  $H$  or  $H'$  individually, Lindblom and Indik [42] define

$$y(r) = r \frac{H'(r)}{H(r)},$$

which gives rise to the first-order differential equation

$$\begin{aligned} \frac{dy}{dr} = & -\frac{y^2}{r} - \frac{r + 4\pi r^3(p - \epsilon)}{r(r-2m)} y \\ & + \frac{4(m + 4\pi r^3 p)^2}{r(r-2m)^2} + \frac{6}{r-2m} - \frac{4\pi r^2}{r-2m} \left[5\epsilon + 9p + \frac{(\epsilon + p)^2}{\epsilon dp/d\epsilon}\right]. \end{aligned} \quad (14)$$

---

<sup>1</sup> Note that, because this gauge does not conform to the constraints of an asymptotically Cartesian and mass-centered chart, there are additional terms in the expansion of the asymptotic metric.

To find  $Y = y(R)$ , we numerically integrate Eq. (14) and evaluate  $y$  at the surface of the star.

Despite appearances, the expression in curly braces in Eq. (13) is  $\mathcal{O}(C^5)$  due to cancellations of terms in curly brackets that are polynomial in  $C$  with terms from the expansion of  $\log(1 - 2C)$ . For stars of small compactness, calculating  $k_2$  directly from Eq. (13) is difficult because it requires that both the numerator and denominator of the right side are accurately calculated to a large number of decimal places. As a result, we expand  $k_2$  to 20 orders in  $C$ . Since  $k_2$  is  $\mathcal{O}(C^0)$ , this allows for much more accurate results for small  $C$ . The compactness has a maximum value of  $1/2$ , so this expansion converges for all stars.

#### D. Estimating the Gravitational Wave Phase Shift due to Tidal Deformability

The tidal deformability  $\lambda$  defined in the last section accurately describes the actual deformation of a neutron star in a binary system only when the neutron star is far from the other compact object. This is for several reasons: As the neutron star approaches the other object, linear perturbation theory and the assumption of a static spacetime used to define  $\lambda$  break down; higher-order multipoles in the metric become important; as the star spirals in, its orbital angular velocity increases and becomes comparable to the frequencies of the star's normal modes, and this enhances the star's response to the tidal perturbation [23]; and, finally, the neutron star may be tidally disrupted before merger. Nevertheless, the tidal deformability turns out essentially to determine the departure of gravitational waveforms from those spinless BBH inspiral in numerical simulations [43–45].

A post-Newtonian expansion [22] describes the effect of tidal deformability on the phase of the gravitational waveform to linear order in  $\lambda$ :

$$\Delta\Phi_{\text{PN}} = -\frac{3\Lambda}{128\eta}(\pi Mf)^{5/3} [a_0 + a_1(\pi Mf)^{2/3}], \quad (15)$$

where  $\Delta\Phi$  is the difference in gravitational wave phase between a spinless BBH and a BHNS binary,  $\Lambda = \lambda/M_{\text{NS}}^5$  is the dimensionless tidal deformability,  $M = M_{\text{BH}} + M_{\text{NS}}$  is the total mass of the binary system,  $\eta = M_{\text{BH}}M_{\text{NS}}/M^2$  is the symmetric mass ratio,  $f$  is the linear

frequency of the gravitational radiation, and  $a_0$  and  $a_1$  are functions of  $\eta$ :

$$a_0 = 12[1 + 7\eta - 31\eta^2 - \sqrt{1 - 4\eta}(1 + 9\eta - 11\eta^2)],$$

$$a_1 = \frac{585}{28} \left[ 1 + \frac{3775}{234}\eta - \frac{389}{6}\eta^2 + \frac{1376}{117}\eta^3 - \sqrt{1 - 4\eta} \left( 1 + \frac{4243}{234}\eta - \frac{6217}{234}\eta^2 - \frac{10}{9}\eta^3 \right) \right].$$

Where Eq. (15) is valid, in the early inspiral when the frequency  $f$  is low, it allows us to easily compute the phase change (the amplitude of the waveform is also affected by tidal deformability, but in this regime the difference in amplitude is negligible). However, tidal effects are largest during late inspiral when the frequency is high.

To extend the analytic computation to late inspiral, Lackey *et al.* [43] fit the amplitude and phase of the gravitational waveforms of neutron star-black hole inspirals to the results of numerical simulations, for black hole spins  $\chi_{\text{BH}}$  between -.5 and .75, and mass ratio  $M_{\text{BH}}/M_{\text{NS}}$  in the range 2 to 5. The resulting expressions (below) depend on post-Newtonian theory for low frequencies, when the neutron star is still far from the black hole. At high frequencies, the fits to numerical results take over:

$$A = \begin{cases} A_{\text{PN}}, & Mf \leq .01 \\ A_{\text{PN}} e^{-\eta \Lambda B(\Lambda, \eta, \chi_{\text{BH}})(Mf - .01)^3}, & Mf > .01 \end{cases} \quad (16)$$

$$\Delta\Phi = \begin{cases} \Delta\Phi_{\text{PN}}(Mf), & Mf \leq .02 \\ -\eta \Lambda E(\eta, \chi_{\text{BH}})(Mf - .02)^{5/3} + \Delta\Phi_{\text{PN}}(.02) + (Mf - .02)\Delta\Phi'_{\text{PN}}(.02), & Mf > .02. \end{cases} \quad (17)$$

Here, subscript *PN* indicates the corresponding result from post-Newtonian theory;  $B$  is a function of  $\Lambda$ ,  $\eta$ , and  $\chi_{\text{BH}}$ ; and  $E$  is a function of  $\eta$  and  $\chi_{\text{BH}}$ . The parameters of  $B$  and  $E$  were determined by the numerical fit. In particular,

$$B = e^{b_0 + b_1\eta + b_2\chi_{\text{BH}}} + \Lambda e^{c_0 + c_1\eta + c_2\chi_{\text{BH}}}$$

with  $\{b_0, b_1, b_2, c_0, c_1, c_2\} = \{-64.985, -2521.8, 555.17, -8.8093, 30.533, 0.6496\}$  as the fitting parameters. Similarly,

$$E = e^{g_0 + g_1\eta + g_2\chi_{\text{BH}} + g_3\eta\chi_{\text{BH}}}$$

with  $\{g_0, g_1, g_2, g_3\} = \{-1.9051, 15.564, -0.41109, 5.7044\}$ . While high tidal deformabilities increase  $|\Delta\Phi|$  relative to a point-particle waveform at a given frequency  $f$ , they also

cause stars to be tidally disrupted earlier in the inspiral, damping the resulting gravitational waves. We define the cutoff frequency  $f_{\text{cutoff}}$  to be the frequency at which effects from tidal deformation dampen the amplitude by a factor of  $e$  relative to the post-Newtonian waveforms. To estimate the total effect of tidal deformability on the phase of the waveform throughout the inspiral, we chose to evaluate  $\Delta\Phi$  at  $f_{\text{cutoff}}$ .

The errors in the fitting parameters reported in [43] correspond to errors in  $\Delta\Phi(Mf_{\text{cutoff}})$  of  $\sim 15\%$  for typical binary parameters. The  $\Delta\Phi$ -values reported below should therefore not be taken as accurate predictions of the tidally-induced phase shift. Still, we expect that applying this fit to the matched causal EOS yields an upper limit on  $|\Delta\Phi|$  with roughly the same error, especially considering the emphasis in [43] on avoiding over-fitting and the lower errors reported for larger  $\Lambda$ -values. A more accurate calculation of the phase shift from BHNS or BNS systems with our causal EOS requires numerical simulations (now in progress for BNS systems [46]) or use of the EOB formalism.

### III. RESULTS

Most neutron stars observed by gravitational waves in binary inspiral are likely to have masses in or near the  $1.25 M_{\odot}$  to  $1.45 M_{\odot}$  range seen in binary neutron star systems, a range consistent with formation from an initial binary of two high-mass stars. We will see that the causal limit on the dimensionless deformability  $\Lambda$  is a monotonically decreasing function of  $M$  and is therefore more stringent for higher mass stars. On the other hand, the fraction of matter above nuclear density is smaller in a low-mass neutron star, and that fact limits the effect of a causal EOS above nuclear density. The net result is that the limit on  $\Lambda$  set by causality is close to the values of  $\Lambda$  associated with candidate neutron-star EOSs for matching densities near nuclear density.

#### A. Effect of Matching Density on Constraints

To understand the results we present in this section, it is helpful first to consider models for which the causal form (2) extends to the surface of the star, where  $p = 0$ . (Here we follow Brecher and Caporaso [32] and Lattimer [33].) That is, we consider models based on

the EOS

$$p = \epsilon - \epsilon_S, \quad (18)$$

and having finite energy density  $\epsilon_S$  at the surface of the star. Because the only dimensionful constant is  $\epsilon_S$ , having (in gravitational units) dimension  $length^{-2}$ , and the mass  $M$  and radius  $R$  each have dimension  $length$ , we have the exact relations

$$M_{\max} \propto \epsilon_S^{-1/2}, \quad R_{\max} \propto \epsilon_S^{-1/2}, \quad (19)$$

where  $R_{\max}$  is the maximum radius among models with central density greater than  $\epsilon_{\text{nuc}}$  (low-density models have larger radii). Because the deformability  $\lambda$  has dimension  $length^5$ , we similarly have

$$\lambda_{\max} \propto \epsilon_S^{-5/2}. \quad (20)$$

Using this truncated causal EOS is equivalent to taking  $\epsilon_S = \epsilon_{\text{match}}$  in the matched causal EOS and discarding the envelope of the star below  $\epsilon_{\text{match}}$ .

For  $\epsilon_{\text{match}} \lesssim \epsilon_{\text{nuc}}$ , where

$$\epsilon_{\text{nuc}} = 2.7 \cdot 10^{14} \text{ g/cm}^3 \quad (21)$$

is nuclear saturation density (the central density of large nuclei), the contribution of the envelope to mass and radius is small enough that the dependence on  $\epsilon_{\text{match}}$  is very nearly the dependence on  $\epsilon_S$  in the truncated star:  $M_{\max}$  and  $R_{\max}$  are each nearly proportional to  $\epsilon_{\text{match}}^{-1/2}$ , and  $\lambda_{\max}$  is nearly proportional to  $\epsilon_{\text{match}}^{-5/2}$ , where  $M_{\max}$  is the maximum neutron-star mass consistent with causality and with a low density EOS below  $\epsilon_{\text{match}}$ ; and  $R_{\max}$  and  $\lambda_{\max}$  are again the corresponding maximum radius and deformability among models with central density greater than  $\epsilon_{\text{nuc}}$ . This behavior can be seen in Figs. 1a and 1b, where linear least-squares fits to the leftmost 10 data points in each plot satisfy

$$M_{\max} = 4.1 M_{\odot} (\epsilon_{\text{match}}/\epsilon_{\text{nuc}})^{-0.4999}, \quad (22a)$$

$$R_{\max} = 17 \text{ km} (\epsilon_{\text{match}}/\epsilon_{\text{nuc}})^{-0.4990}, \quad (22b)$$

$$\lambda_{\max} = (1.3 \cdot 10^{37} \text{ g cm}^2 \text{ s}^2) (\epsilon_{\text{match}}/\epsilon_{\text{nuc}})^{-2.4996}. \quad (22c)$$

The rightmost data points in each plot diverge from the line because, at higher matching densities, a larger envelope obeys the low-density (MS1) EOS.

Of greater astrophysical relevance than the upper limit on  $\lambda$ , however, is the constraint on the dimensionless tidal deformability,  $\Lambda = \lambda/M_{\text{NS}}^5 = \frac{2}{3} k_2 R^5/M^5$ , that governs the waveform

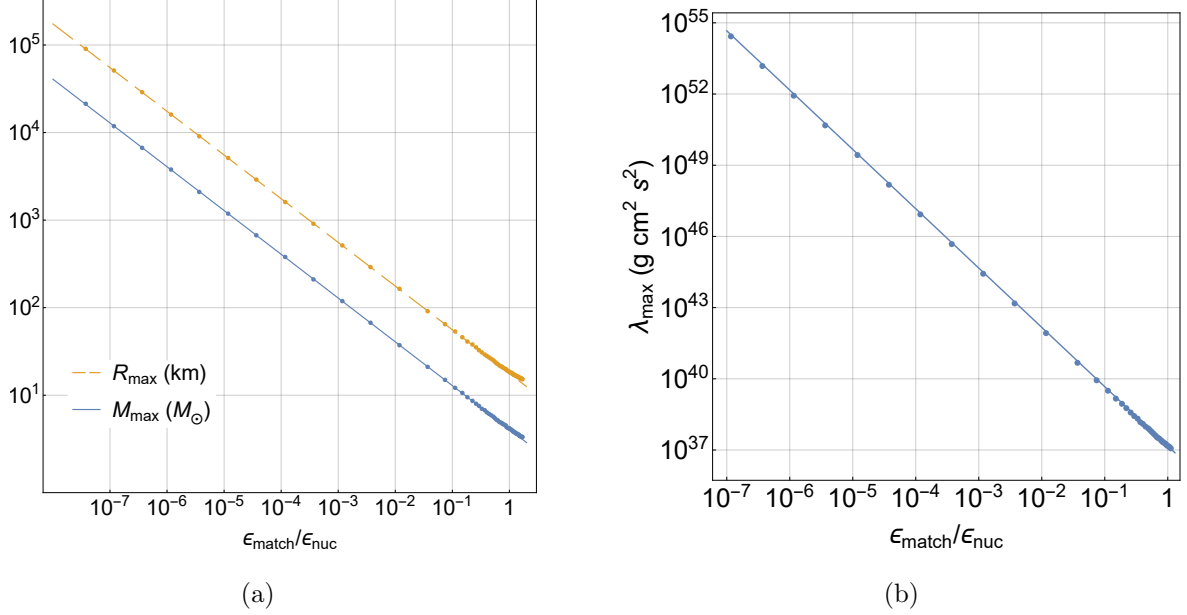


FIG. 1. The (a) the maximum radius, mass, and (b) tidal deformability are plotted against the matching density. The behavior of all three quantities follow a power law except at high  $\epsilon_{\text{match}}$ , with the best-fit lines given by Eq. (22)

of a binary inspiral. As we will see below, because of the factor  $M_{\text{NS}}^{-5}$ ,  $\Lambda$  is monotonically decreasing with increasing mass for central density above  $\epsilon_{\text{match}}$ . The physically interesting constraint on  $\Lambda$  is then a constraint at known mass: Inspiral waveforms detected with a high enough signal-to-noise ratio to measure their tidal departure from point-particle inspiral will also have the most accurately measured neutron-star masses. The dependence of  $\Lambda$  on  $\epsilon_{\text{match}}$  for fixed mass cannot be found from the previous dimensional analysis, but it is easy to see that  $\Lambda(M, \epsilon_{\text{match}})$  is a monotonically decreasing function of  $\epsilon_{\text{match}}$ : As  $\epsilon_{\text{match}}$  increases and less of the star is governed by the stiffer causal EOS, the star becomes more compact:  $R$  decreases at fixed  $M$ . In addition, as the density profile becomes more centrally condensed, the tidal Love number  $k_2$  decreases, because, for a given radius, the external tidal force has less effect on a more centrally condensed star. Decreasing  $R$  and  $k_2$  gives a sharp decrease in  $\Lambda$ , as shown in Fig. 2 for a  $1.4M_{\odot}$  star. For  $.33\epsilon_{\text{nuc}} < \epsilon_{\text{match}} < 1.2\epsilon_{\text{nuc}}$  we find a near power-law dependence,

$$\Lambda_{1.4} = 2400(\epsilon_{\text{match}}/\epsilon_{\text{nuc}})^{-1.8}. \quad (23)$$

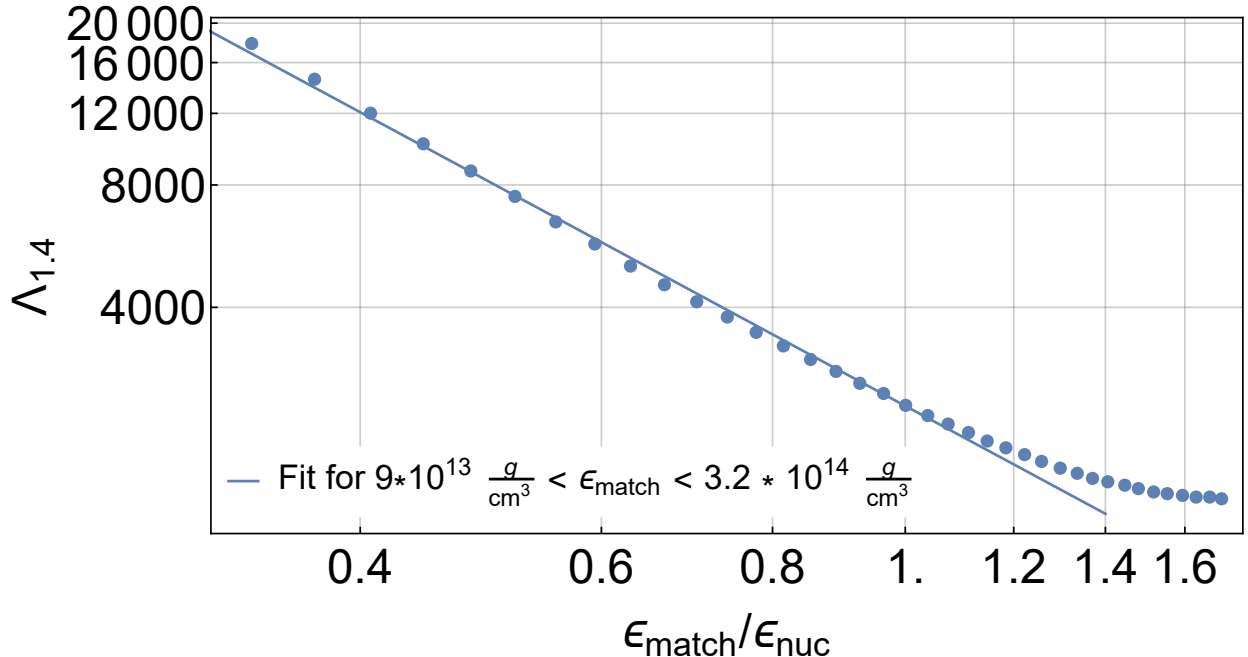


FIG. 2. The dependence of the dimensionless tidal deformability  $\Lambda_{1.4}$  of  $1.4M_{\odot}$  stars on matching density is shown on a log-log plot. The behavior approximates a power law for  $\epsilon \lesssim \epsilon_{\text{nuc}}$ , with the best fit given by Eq. (23).

### B. Comparison between Constraint and Results from Candidate EOSs

We begin by displaying the limit set by causality on the dimensionful tidal deformability  $\lambda$  as a function of mass, with  $\epsilon_{\text{match}}$  taken to be  $\epsilon_{\text{nuc}}$ . As noted earlier, there is remaining uncertainty in the equation of state at  $\epsilon_{\text{nuc}}$ , and we obtain a conservative upper limit by matching to the MS1 EOS [35], which is particularly stiff at low densities.

The mass-radius relation for the family of neutron stars obeying the matched causal EOS is indicated by “Matched Causal” in Fig. 3(a). As we saw in Eqs. (22), matching to MS1 below  $\epsilon_{\text{nuc}}$  is a weak constraint, giving  $M_{\text{max}} = 4.1M_{\odot}$  and  $R_{\text{max}} > 18$  km, both significantly larger than their values for any of the candidate EOSs shown. These candidate EOSs include SLy [47], which is one of the softest EOSs that allow for  $2M_{\odot}$  neutron stars, MPA1 [48], which is slightly stiffer, H4 [49], which is stiff at low densities and soft at high densities, and MS1 [35], which is particularly stiff at all densities. The maximum masses allowed by these EOSs are all between 2 and  $2.8 M_{\odot}$ , and the radii are all between 10 and 15 km.

In Figure 3(b), the top curve displays an upper limit on  $\lambda$  as a function of neutron-

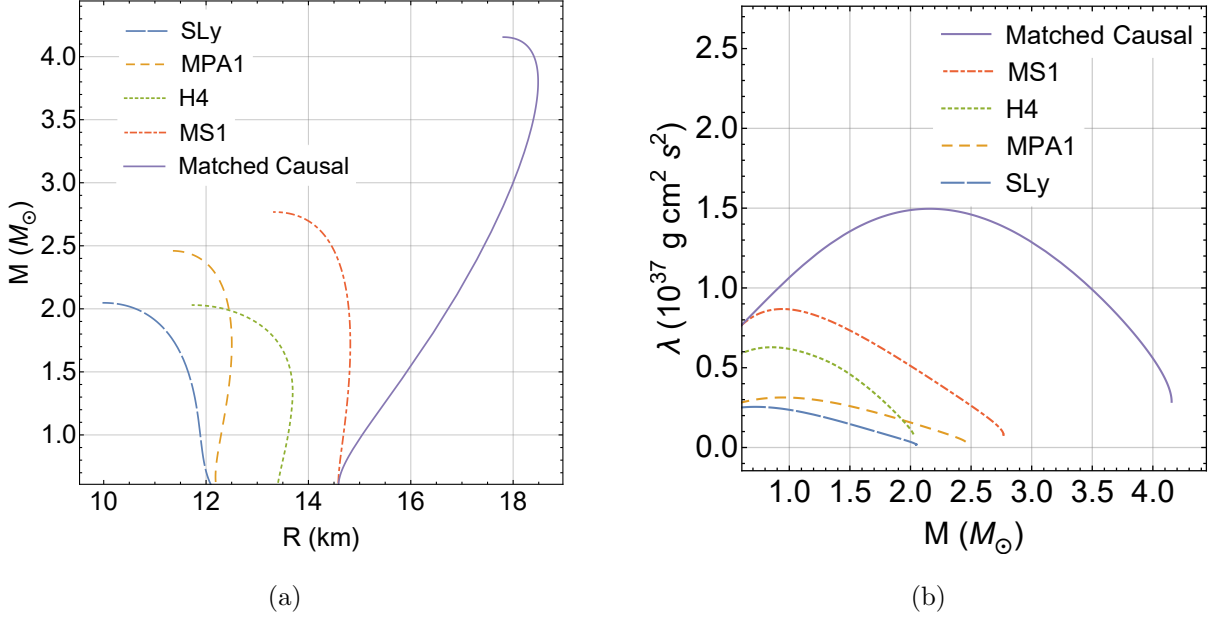


FIG. 3. (a) The mass-radius relation for the matched causal EOS with  $\epsilon_{\text{match}} = \epsilon_{\text{nuc}}$  and for candidate neutron-star equations of state that display the range of uncertainty in stiffness.

(b) Tidal deformability versus mass for stars based on the same EOSs. The top solid curve, displaying the tidal deformability of stars based on the matched causal EOS, is an upper limit set by causality on tidal deformability. Stars based on softer EOSs have smaller tidal deformabilities.

star mass obtained from the matched causal EOS. The comparison  $\lambda(M)$  curves for the same candidate EOSs of Fig. 3(a) show the decreasing deformability associated with stars of decreasing stiffness and radius. Note, however, that the maximum value of  $\lambda$  for each EOS occurs at a smaller mass than that of the model with maximum radius. This is due to the increase in central condensation as the mass increases, resulting in an decrease in  $k_2$ . The maximum of the  $\lambda(M)$  curve for the matched causal EOS gives the mass-independent upper limit  $\lambda < 1.5 \times 10^{37} g cm^2 s^2$ , for  $\epsilon_{\text{match}} = \epsilon_{\text{nuc}}$ , with dependence on  $\epsilon_{\text{match}}$  given by Eq. (22c) for smaller matching density.

The corresponding upper limit  $\Lambda_{\text{max}}(M)$  on the dimensionless deformability is given by the top curve in Fig. 4, for  $\epsilon_{\text{match}} = \epsilon_{\text{nuc}}$ . (The dependence on  $\epsilon_{\text{match}}$  was shown in Fig. 2 for a representative  $1.4 M_{\odot}$  star.) Since  $\Lambda \propto C^{-5}$ ,  $\Lambda$  is large for small masses and relatively small for larger masses. As a result, it is not meaningful to speak of a mass-independent maximum of  $\Lambda$ , but it is meaningful to compare  $\Lambda$ -values at constant mass. The most striking feature of Fig. 4 is how close the curve  $\Lambda_{\text{max}}(M)$  is to the range of  $\Lambda$  allowed by

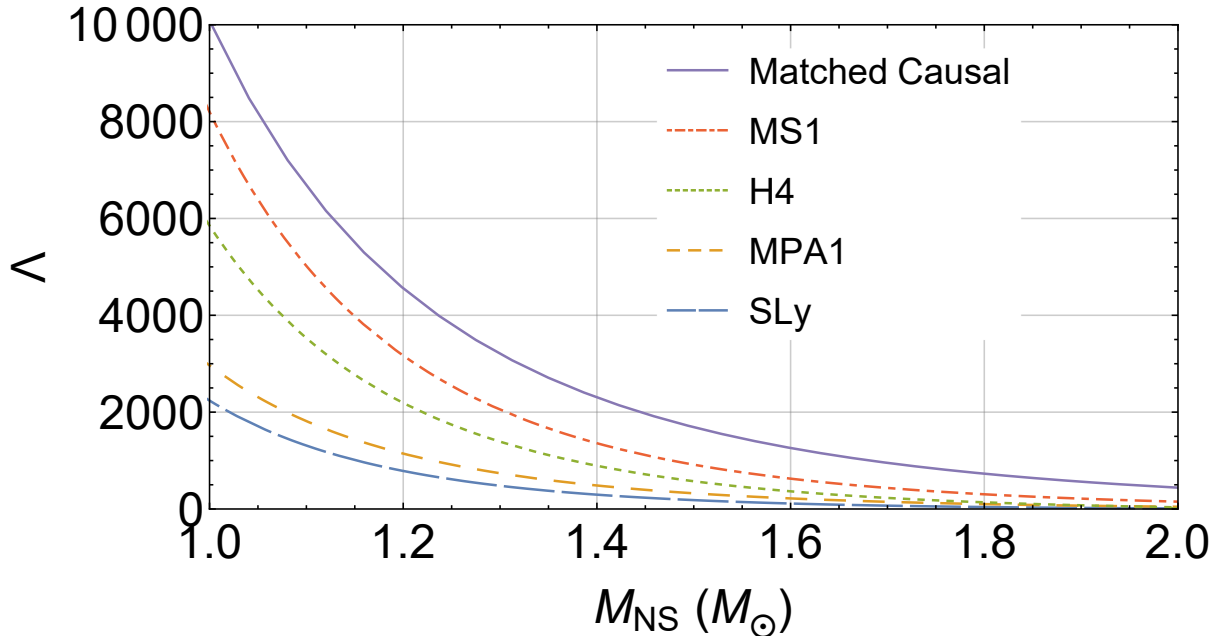


FIG. 4. The dimensionless tidal deformability  $\Lambda$  is plotted against mass for several EOSs. For any given mass, the Matched Causal EOS places an upper limit on the value of  $\Lambda$ .

current candidate EOSs. This stringent constraint on  $\Lambda$  is in sharp contrast to the larger departures of the curves giving  $R_{\text{max}}(M)$  and  $\lambda_{\text{max}}(M)$  in Fig. 3 from the corresponding curves for candidate EOSs. For  $1.4 M_{\odot}$  stars, for example, it places the constraint that  $\Lambda \leq 2300$ . For comparison,  $1.4 M_{\odot}$  stars resulting from the SLy, MPA1, H4, and MS1 EOSs have  $\Lambda$ -values of 300, 490, 900, and 1400, respectively.

One might naively expect  $|\Delta\Phi(f_{\text{cutoff}})|$  to increase monotonically with  $\Lambda$  and therefore to decrease monotonically with the mass  $M_{\text{NS}}$  of the neutron star. This is not the case, because while  $|\Delta\Phi|$  increases with  $\Lambda$  (and decreases with  $M_{\text{NS}}$ ) when evaluated at a fixed frequency,  $f_{\text{cutoff}}$  decreases monotonically with  $\Lambda$  (and increases monotonically with  $M_{\text{NS}}$ ). That is, stars with high dimensionless tidal deformability are tidally disrupted at a larger distance from the black hole, corresponding to a smaller orbital (and gravitational wave) frequency. A neutron star with high tidal deformability therefore has fewer cycles during which to accumulate phase relative to a point-particle. As a result, the effect of  $M_{\text{NS}}$  on  $|\Delta\Phi(f_{\text{cutoff}})|$  is complicated, and depends on EOS and the parameters of the binary.

Nevertheless, stiffer EOSs result in larger values of  $|\Delta\Phi|$  for given neutron star masses or mass ratios. As can be seen in Fig. 5,  $|\Delta\Phi(f_{\text{cutoff}})|$  decreases with mass ratio for all EOSs

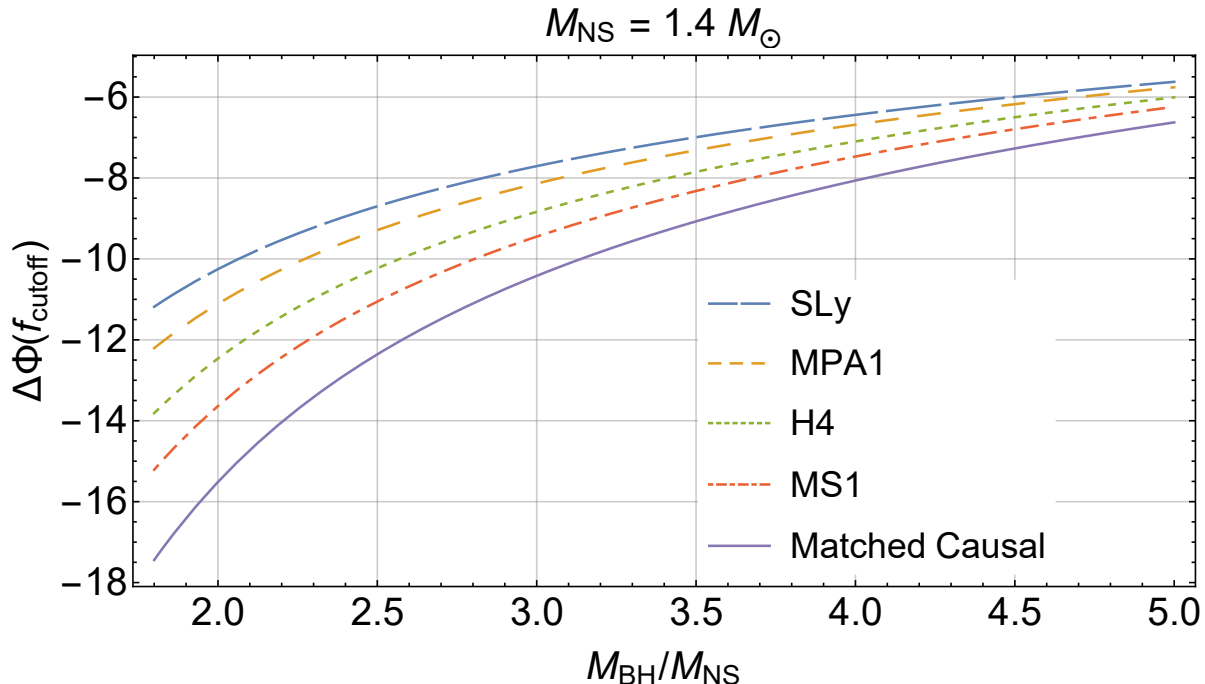


FIG. 5. The estimated total gravitational wave phase shift  $\Delta\Phi(f_{\text{cutoff}})$  corresponding to a BHNS binary with  $M_{\text{NS}} = 1.4 M_{\odot}$  and  $\chi_{\text{BH}} = 0$  is plotted against the mass ratio for several EOSs. For a given mass ratio,  $|\Delta\Phi(f_{\text{cutoff}})|$  is larger for stiffer EOSs, and the Matched Causal EOS provides a constraint on it. In general,  $|\Delta\Phi(f_{\text{cutoff}})|$  decreases with the mass ratio.

(note that, although  $\Delta\Phi$  is positive when evaluated at a given time, it is negative when evaluated at a given frequency). On the other hand,  $|\Delta\Phi(f_{\text{cutoff}})|$  has complicated behavior with respect to neutron star mass for all EOSs when the spin of the companion black hole is zero (Fig. 6). In addition, one can see in Fig. 5 and Fig. 6 that  $|\Delta\Phi(f_{\text{cutoff}})|$  increases with the stiffness of the EOS, and is largest for our EOS, but only by a few radians at most. Here, based on our estimate of  $\Delta\Phi$ , the constraint set by causality is remarkably strong, stronger than the already stringent constraint on  $\Lambda$ :  $\Delta\Phi_{\text{max}}(M)$  differs from its value for the stiffest candidate equation of state by less than 14%. The strength of the causal constraint is due to (a) the fact that  $\Lambda$  is largest at small mass, where the causal EOS governs the smallest fraction of the star, and (b) a larger cutoff frequency for the stiffest equations of state that reduces the time over which the phase can accumulate.

As shown in Fig. 7, for a given black hole mass  $M_{\text{BH}}$  and zero black hole spin  $\chi_{\text{BH}}$ ,  $|\Delta\Phi(f_{\text{cutoff}})|$  increases with  $M_{\text{NS}}$  for the Matched Causal EOS. In addition, for a given  $M_{\text{NS}}$ ,  $|\Delta\Phi(f_{\text{cutoff}})|$  decreases with  $M_{\text{BH}}$ . Changing  $\chi_{\text{BH}}$  can change the qualitative behavior of

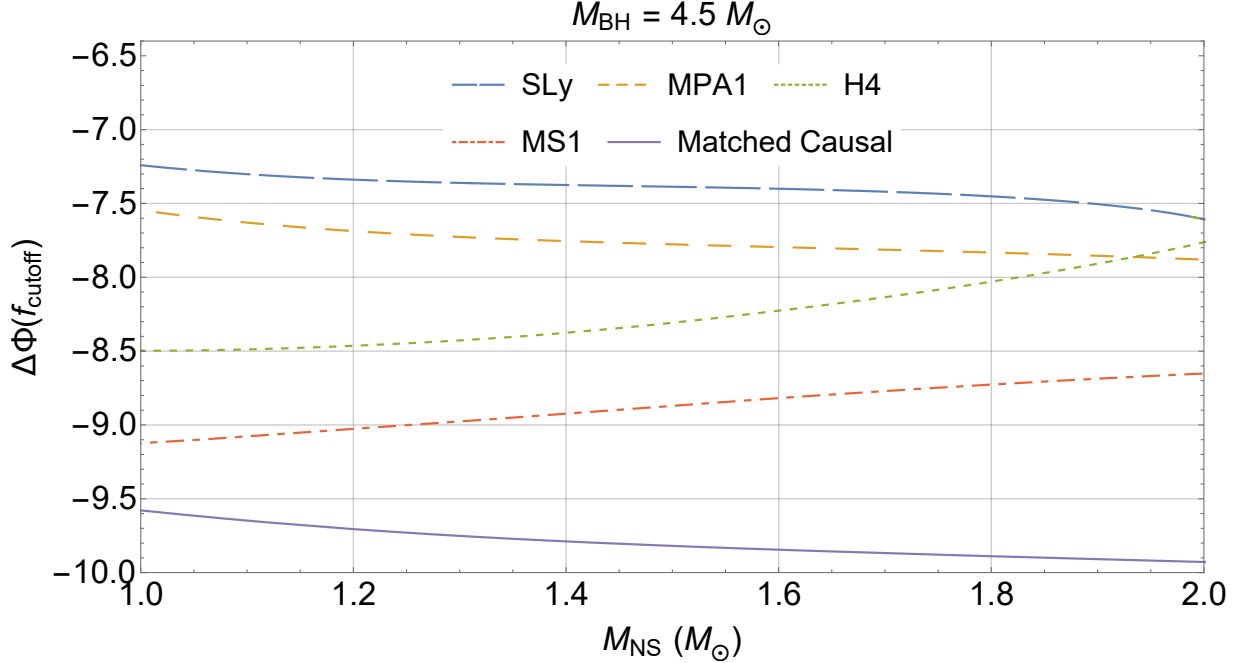


FIG. 6. The estimated total gravitational wave phase shift  $\Delta\Phi(f_{\text{cutoff}})$  corresponding to a BHNS binary with  $M_{BH} = 4.5 M_{\odot}$  and  $\chi_{BH} = 0$  is plotted against neutron star mass for several EOSs. For a given mass,  $|\Delta\Phi(f_{\text{cutoff}})|$  is larger for stiffer EOSs, and the Matched Causal EOS provides a constraint on it. The dependence of  $|\Delta\Phi(f_{\text{cutoff}})|$  on neutron star mass is complicated and changes with the EOS used.

$|\Delta\Phi(f_{\text{cutoff}})|$ , as can be seen in Fig. 8. In particular, a corotating companion black hole tends to make  $|\Delta\Phi(f_{\text{cutoff}})|$  increase with mass, while antirotating companions tend to make  $|\Delta\Phi(f_{\text{cutoff}})|$  decrease with mass. For a given  $M_{NS}$ , higher (corotating) spins result in smaller  $|\Delta\Phi(f_{\text{cutoff}})|$ , but the effect decreases with increasing  $M_{NS}$ .

Figure 9 shows how  $|\Delta\Phi(f_{\text{cutoff}})|$  varies with mass ratio for several neutron star masses and 0 black hole spin. For a given  $M_{NS}$ ,  $|\Delta\Phi(f_{\text{cutoff}})|$  decreases with increasing mass ratio. For a given mass ratio,  $|\Delta\Phi(f_{\text{cutoff}})|$  decreases with neutron star mass. The effect decreases in magnitude as the mass ratio increases.

Finally, Fig. 10 shows  $|\Delta\Phi(f_{\text{cutoff}})|$  varying with mass ratio for several black hole spins and  $M_{NS} = 1.4 M_{\odot}$ .  $|\Delta\Phi(f_{\text{cutoff}})|$  decreases with mass ratio regardless of the value of  $\chi_{BH}$ , but for a given mass ratio,  $|\Delta\Phi(f_{\text{cutoff}})|$  decreases with  $\chi_{BH}$ ; it is smallest for corotating black holes, and largest for antirotating black holes.

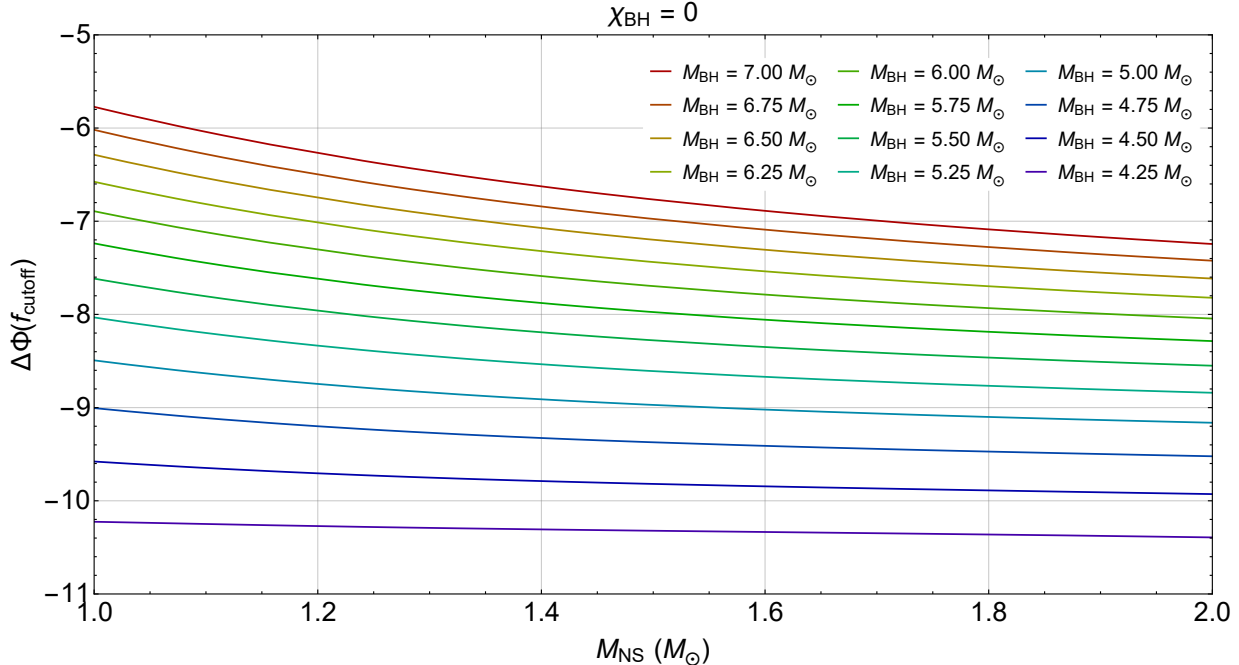


FIG. 7. The estimated constraint on  $\Delta\Phi(f_{\text{cutoff}})$  is plotted against the mass of a neutron star for several different black hole masses and a black hole spin of 0. We expect that the absolute value of  $\Delta\Phi$  would be lower for any real BHNS binary. The constraint on  $|\Delta\Phi|$  decreases with both neutron star mass and black hole mass.

#### IV. CONCLUSION

By using a stiffest causal EOS consistent with causality at high density, matched to the MS1 [35] EOS below a density  $\epsilon_{\text{match}}$ , we have set upper limits on the quadrupole tidal deformability  $\lambda$  and on the dimensionless tidal deformability  $\Lambda$  as a function of neutron star mass. The limit on  $\Lambda$ , given by Eq. (23) for a  $1.4 M_{\odot}$  neutron star, is conservative, because we have matched to an EOS (MS1) that is stiff below nuclear density: With this low-density EOS and a match at  $\epsilon_{\text{nuc}}$ , the corresponding upper mass limit is  $4.1M_{\odot}$ . Using the constraint on dimensionless tidal deformability and the Lackey *et al.* analytic fit to numerical data [43], we then estimated the induced phase shift of a BHNS inspiral and merger waveform.

The implied upper limit on the accumulated phase shift  $|\Delta\Phi|$  at merger depends on the parameters of the binary, but it is surprisingly close to the range of phase shifts seen in candidate EOSs. Assuming one can neglect resonant interactions of the tidal field with neutron-star modes, we think this conclusion is secure. We emphasize, however, that our

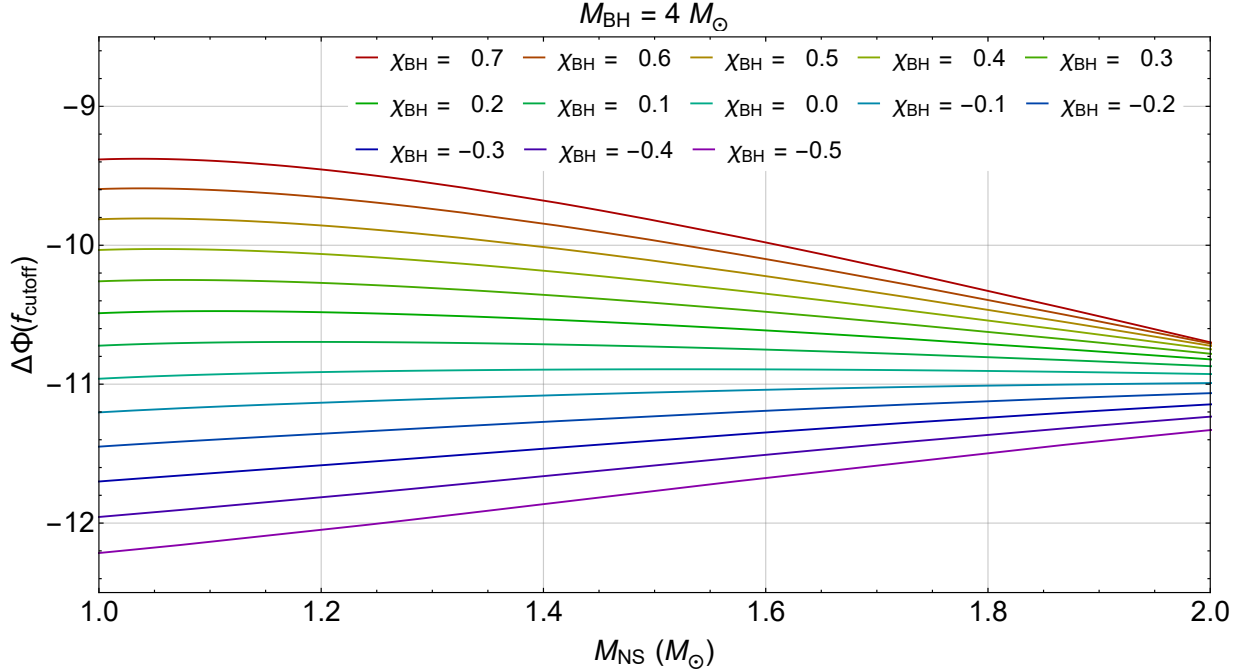


FIG. 8. The estimated constraint on  $\Delta\Phi(f_{\text{cutoff}})$  is plotted against the mass of a neutron star for several different black hole spins and a black hole mass of  $4M_{\odot}$ . Different black hole spins can change how  $\Delta\Phi$  qualitatively changes with neutron star mass, and  $\Delta\Phi$  depends more strongly on  $\chi_{\text{BH}}$  for smaller neutron star masses than for larger neutron star masses.

upper limits on  $|\Delta\Phi|$  rely on an analytic expression based on full numerical simulations for models with a set of EOSs significantly less stiff than the matched causal EOS. Work *has* begun on numerical simulations to obtain an upper limit on the departure of double neutron star inspiral waveforms from the point-particle (or spinless BBH) case.

## ACKNOWLEDGMENTS

We would like to thank Benjamin Lackey and Lee Lindblom for sharing data with us and Lindblom for a useful discussion regarding multiple-parameter EOSs. This work was supported in part by NSF Grant Nos. PHY-1307429 and PHY-1607585.

- 
- [1] C. S. Kochanek, *The Astrophysical Journal* **398**, 234 (1992).
  - [2] D. Lai and A. G. Wiseman, *Physical Review D* **54**, 3958 (1996).

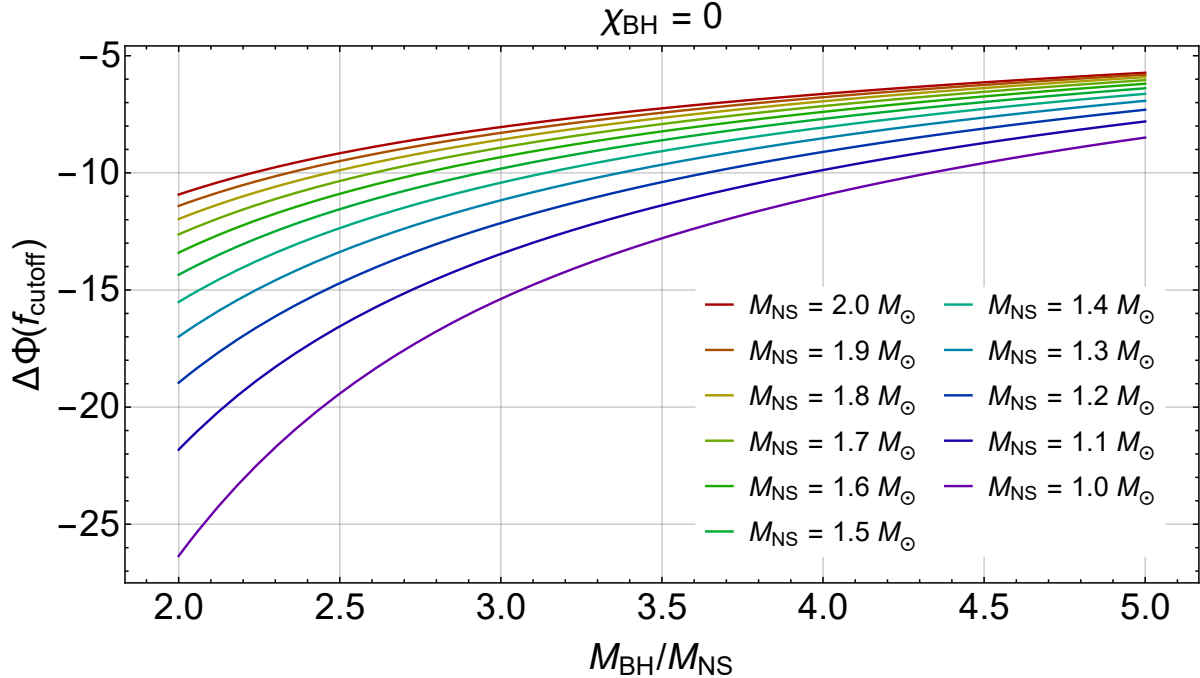


FIG. 9. The estimated constraint on  $|\Delta\Phi(f_{\text{cutoff}})|$  for BHNS binaries with  $\chi_{BH} = 0$  is plotted against the mass ratio for several neutron star masses.  $|\Delta\Phi(f_{\text{cutoff}})|$  decreases both with mass ratio and with neutron star mass.

- [3] F. Pannarale, E. Berti, K. Kyutoku, B. D. Lackey, and M. Shibata, Phys. Rev. D **92**, 084050 (2015).
- [4] K. Chatziioannou, K. Yagi, A. Klein, N. Cornish, and N. Yunes, Phys. Rev. D **92**, 104008 (2015), arXiv:1508.02062 [gr-qc].
- [5] X. Zhuge, J. M. Centrella, and S. L. McMillan, Physical Review D **54**, 7261 (1996).
- [6] K. Uryū, M. Shibata, and Y. Eriguchi, Physical Review D **62**, 104015 (2000).
- [7] J. A. Faber, P. Grandclément, F. A. Rasio, and K. Taniguchi, Physical review letters **89**, 231102 (2002).
- [8] J. A. Faber, P. Grandclément, and F. A. Rasio, Physical Review D **69**, 124036 (2004).
- [9] M. Bejger, D. Gondek-Rosińska, E. Gourgoulhon, P. Haensel, K. Taniguchi, and J. Zduńnik, Astronomy & Astrophysics **431**, 297 (2005).
- [10] D. Gondek-Rosińska, M. Bejger, T. Bulik, E. Gourgoulhon, P. Haensel, F. Limousin, K. Taniguchi, and L. Zduńnik, Advances in Space Research **39**, 271 (2007).
- [11] M. Shibata, K. Taniguchi, and K. Uryū, Physical Review D **71**, 084021 (2005).

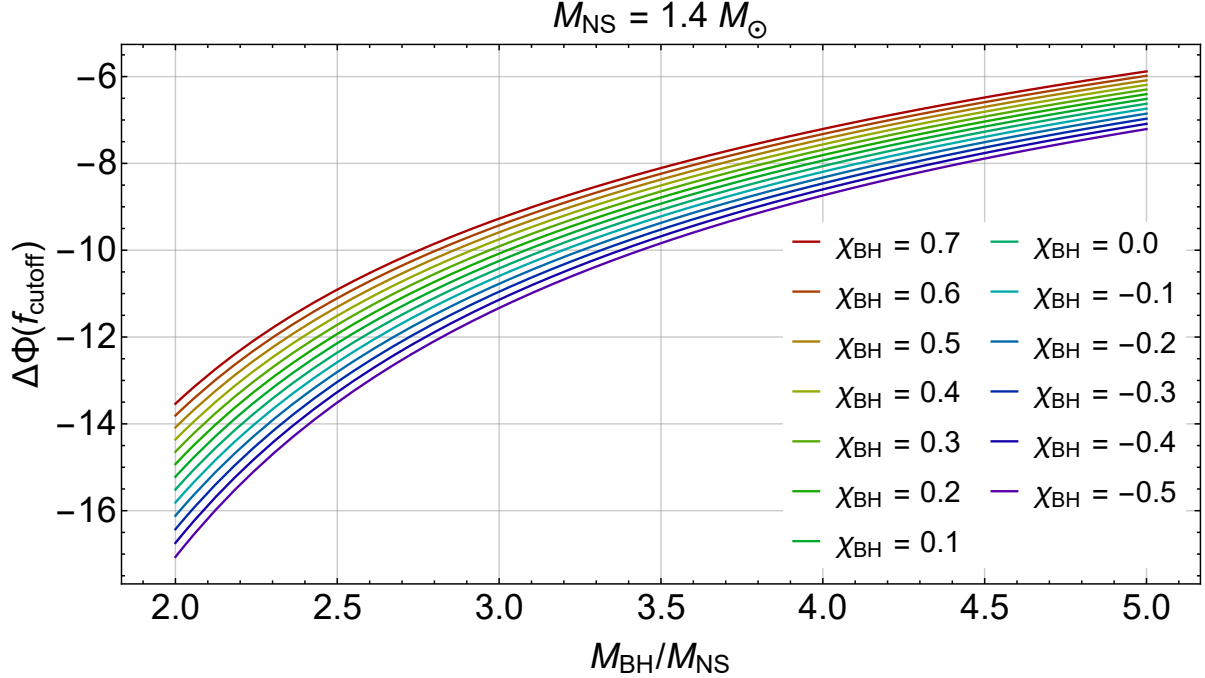


FIG. 10. The estimated constraint on  $|\Delta\Phi(f_{\text{cutoff}})|$  for BHNS binaries with  $M_{NS} = 1.4 M_{\odot}$  is plotted against the mass ratio for several black hole spins. The value of  $|\Delta\Phi(f_{\text{cutoff}})|$  decreases with mass ratio and with spin.

- [12] M. Shibata and K. Uryū, *Progress of Theoretical Physics* **107**, 265 (2002).
- [13] R. Oechslin and H.-T. Janka, *Physical review letters* **99**, 121102 (2007).
- [14] K. Taniguchi and E. Gourgoulhon, *Physical Review D* **68**, 124025 (2003).
- [15] M. Shibata, *Physical Review D* **60**, 104052 (1999).
- [16] M. Shibata and K. Uryū, *Physical Review D* **61**, 064001 (2000).
- [17] M. Shibata and K. Taniguchi, *Physical Review D* **73**, 064027 (2006).
- [18] M. Shibata, K. Taniguchi, and K. Uryū, *Physical Review D* **68**, 084020 (2003).
- [19] M. Miller, P. Gressman, and W.-M. Suen, *Physical Review D* **69**, 064026 (2004).
- [20] P. Marronetti, M. D. Duez, S. L. Shapiro, and T. W. Baumgarte, *Physical review letters* **92**, 141101 (2004).
- [21] Y. T. Liu, S. L. Shapiro, Z. B. Etienne, and K. Taniguchi, *Physical Review D* **78**, 024012 (2008).
- [22] J. Vines, É. É. Flanagan, and T. Hinderer, *Physical Review D* **83**, 084051 (2011).
- [23] T. Hinderer, A. Taracchini, F. Foucart, A. Buonanno, J. Steinhoff, M. Duez, L. E. Kidder,

- H. P. Pfeiffer, M. A. Scheel, B. Szilagyi, *et al.*, Physical review letters **116**, 181101 (2016).
- [24] S. Bernuzzi, T. Dietrich, and A. Nagar, Physical Review Letters **115**, 091101 (2015), arXiv:1504.01764 [gr-qc].
- [25] S. Bernuzzi, A. Nagar, T. Dietrich, and T. Damour, Physical Review Letters **114**, 161103 (2015), arXiv:1412.4553 [gr-qc].
- [26] K. Hotokezaka, K. Kyutoku, Y.-i. Sekiguchi, and M. Shibata, Phys. Rev. D **93**, 064082 (2016), arXiv:1603.01286 [gr-qc].
- [27] T. Damour, A. Nagar, and L. Villain, Physical Review D **85**, 123007 (2012).
- [28] W. Del Pozzo, T. G. Li, M. Agathos, C. Van Den Broeck, and S. Vitale, Physical review letters **111**, 071101 (2013).
- [29] M. Agathos, J. Meidam, W. Del Pozzo, T. G. F. Li, M. Tompitak, J. Veitch, S. Vitale, and C. Van Den Broeck, Phys. Rev. D **92**, 023012 (2015), arXiv:1503.05405 [gr-qc].
- [30] L. Wade, J. D. Creighton, E. Ochsner, B. D. Lackey, B. F. Farr, T. B. Littenberg, and V. Raymond, Physical Review D **89**, 103012 (2014).
- [31] C. E. Rhoades Jr and R. Ruffini, Physical Review Letters **32**, 324 (1974).
- [32] K. Brecher and G. Caporaso, Nature **259**, 377 (1976).
- [33] J. M. Lattimer, Annual Review of Nuclear and Particle Science **62**, 485 (2012), arXiv:1305.3510 [nucl-th].
- [34] R. Geroch and L. Lindblom, Annals of Physics **207**, 394 (1991).
- [35] H. Mueller and B. D. Serot, Nuclear Physics A **606**, 508 (1996).
- [36] P. Pani, L. Gualtieri, A. Maselli, and V. Ferrari, Phys. Rev. D **92**, 024010 (2015), arXiv:1503.07365 [gr-qc].
- [37] R. Essick, S. Vitale, and N. N. Weinberg, Phys. Rev. D **94**, 103012 (2016), arXiv:1609.06362 [astro-ph.HE].
- [38] J. R. Oppenheimer and G. M. Volkoff, Physical Review **55**, 374 (1939).
- [39] É. É. Flanagan and T. Hinderer, Physical Review D **77**, 021502 (2008).
- [40] T. Hinderer, The Astrophysical Journal **677**, 1216 (2008).
- [41] T. Regge and J. A. Wheeler, Physical Review **108**, 1063 (1957).
- [42] L. Lindblom and N. M. Indik, Physical Review D **89**, 064003 (2014).
- [43] B. D. Lackey, K. Kyutoku, M. Shibata, P. R. Brady, and J. L. Friedman, Physical Review D **89**, 043009 (2014).

- [44] B. D. Lackey, K. Kyutoku, M. Shibata, P. R. Brady, and J. L. Friedman, *Phys. Rev. D* **85**, 044061 (2012), arXiv:1109.3402 [astro-ph.HE].
- [45] J. S. Read, L. Baiotti, J. D. E. Creighton, J. L. Friedman, B. Giacomazzo, K. Kyutoku, C. Markakis, L. Rezzolla, M. Shibata, and K. Taniguchi, *Phys. Rev. D* **88**, 044042 (2013), arXiv:1306.4065 [gr-qc].
- [46] C. Markakis *et al.*, (in preparation).
- [47] F. Douchin and P. Haensel, *Astronomy & Astrophysics* **380**, 151 (2001).
- [48] H. Mütter, M. Prakash, and T. Ainsworth, *Physics Letters B* **199**, 469 (1987).
- [49] B. D. Lackey, M. Nayyar, and B. J. Owen, *Physical Review D* **73**, 024021 (2006).
- [50] A. Lichnerowicz, *Applications of Nonlinear Partial Differential Equations in Mathematical Physics: Proceedings of Symposia in Applied Mathematics*, **17**, 189 (1965).
- [51] W. Israel, *Annals of Physics* **100**, 310 (1976).
- [52] W. Israel and J. M. Stewart, *Annals of Physics* **118**, 341 (1979).
- [53] I.-S. Liu, I. Müller, and T. Ruggeri, *Annals of Physics* **169**, 191 (1986).
- [54] A. Reisenegger and P. Goldreich, *Astrophys. J.* **395**, 240 (1992).

### Appendix A: Comments on causality

With the assumption that the equilibrium equation of state of the neutron star and its perturbations are governed by the same one-parameter equation of state, causality implies  $dp/d\epsilon < 1$ . That is, as mentioned in the text, the time-evolution of a barotropic fluid is described by a hyperbolic system whose characteristics lie within the light cone precisely when  $dp/d\epsilon < 1$  [50]. The frequencies of stellar perturbations, however, are too high for the temperature of a fluid element and the relative density  $Y_i$  of each species of particle to reach their values for the background fluid at the same pressure: Heat flow and nuclear reactions are incomplete.

Because of this, one cannot precisely identify the maximum speed of signal propagation in the fluid with the equilibrium value

$$\sqrt{\left. \frac{dp}{d\epsilon} \right|_{\text{equilibrium}}} := \sqrt{\frac{dp/dr}{d\epsilon/dr}}.$$

If short wavelength, high frequency perturbations are too rapid for heat flow and for nuclear

reactions to proceed, their speed of propagation is

$$v_{\text{sound}} = \sqrt{(\partial p / \partial \epsilon)|_{s, Y_i}}. \quad (\text{A1})$$

One therefore expects causality to imply

$$\left. \frac{\partial p}{\partial \epsilon} \right|_{s, Y_i} < 1. \quad (\text{A2})$$

This is known to be true for a relativistic fluid with a two-parameter EOS of the form  $p = p(\epsilon, s)$ : Its dynamical evolution then involves heat flow and is governed by the equations of a dissipative relativistic fluid. Causal theories of this kind were first introduced by Israel and Stewart [51, 52] and by Liu *et al.* [53]. The general class of such theories was analyzed by Geroch and Lindblom [34], who pointed out that, for dissipative fluids obeying  $p = p(\epsilon, s)$ , causality implies the inequality (A2),

$$\left. \frac{\partial p}{\partial \epsilon} \right|_s < 1. \quad (\text{A3})$$

Now a star is unstable to convection if

$$\left. \frac{dp}{d\epsilon} \right|_{\text{equilibrium}} > \left. \frac{\partial p}{\partial \epsilon} \right|_{s, Y_i}. \quad (\text{A4})$$

Thus, *for a locally stable spherical star (a self-gravitating equilibrium configuration of a relativistic dissipative fluid) based on a two-parameter EOS  $p = p(\epsilon, s, Y_i)$ , causality implies*

$$\sqrt{\left. \frac{dp}{d\epsilon} \right|_{\text{equilibrium}}} < 1. \quad (\text{A5})$$

For a dissipative fluid obeying a multi-parameter EOS of the form  $p = p(\epsilon, s, Y_i)$ , we are not aware of a general proof that causality implies the inequality (A2). One has only the weaker statement, *for a locally stable spherical star based on an EOS equation of state  $p = p(\epsilon, s)$ ,  $v_{\text{sound}} < 1$  implies the equilibrium inequality (A5).*

Although the inequality  $v_{\text{sound}} < 1$  is stronger than the the equilibrium inequality (A5) used to place upper limits on mass, radius and, in the present paper, on deformability, the difference is small. The fractional difference

$$\frac{\sqrt{dp/d\epsilon|_{\text{equilibrium}}} - \sqrt{(\partial p)/(\partial \epsilon)|_{s, Y_i}}}{\sqrt{(\partial p)/(\partial \epsilon)|_{s, Y_i}}} \quad (\text{A6})$$

is primarily due to composition (to the constant values of  $Y_i$ ), and it is less than 5%. (It is approximately half the fractional difference between the adiabatic index  $\gamma = \Gamma_1$  and the

index  $\Gamma$  governing the equilibrium configuration; the difference determines the Brunt-Väisälä frequency, a characteristic frequency of  $g$ -modes, and an estimate can be found, for example, in Ref. [54].)